PNAS RESEARCH ARTICLE | APPLIED PHYSICAL SCIENCES

Small field chaos in spin glasses: Universal predictions from the ultrametric tree and comparison with numerical simulations

Miguel Aguilar-Janita[a,1], Silvio Franz[b], Victor Martin-Mayor[c], Javier Moreno-Gordo[d,e,f,g], Giorgio Parisi[h,1], Federico Ricci-Tersenghi[h], and Juan J. Ruiz-Lorenzo[f,g]

Affiliations are included on p. 7.

Contributed by Giorgio Parisi; received March 14, 2024; accepted July 29, 2024; reviewed by Stefan Boettcher and Koji Hukushima

Replica symmetry breaking (RSB) for spin glasses predicts that the equilibrium configuration at two different magnetic fields are maximally decorrelated. We show that this theory presents quantitative predictions for this chaotic behavior under the application of a vanishing external magnetic field, in the crossover region where the field intensity scales proportionally to $1/\sqrt{N}$, being N the system size. We show that RSB theory provides universal predictions for chaotic behavior: They depend only on the zero-field overlap probability function $P(q)$ and are independent of other system features. In the infinite volume limit, each spin-glass sample is characterized by an infinite number of states that have a tree-like structure. We generate the corresponding probability distribution through efficient sampling using a representation based on the Bolthausen–Sznitman coalescent. Using solely $P(q)$ as input we can analytically compute the statistics of the states in the region of vanishing magnetic field. In this way, we can compute the overlap probability distribution in the presence of a small vanishing field and the increase of chaoticity when increasing the field. To test our computations, we have simulated the Bethe lattice spin glass and the 4D Edwards–Anderson model, finding in both cases excellent agreement with the universal predictions.

replica symmetry breaking | Edwards–Anderson model | Bethe lattice | Bolthausen–Sznitman coalescent

Significance

There are many numerical models and experimental systems supposedly described by the Replica Symmetry Breaking theory. Unfortunately, usually, the predictions of the theory are only qualitative, with the notable exception of the modified fluctuation-dissipation relations. We improve this situation by finding a quantitative description of the chaotic behavior that occurs upon varying the magnetic field in the region of very small fields. We provide a detailed comparison of our analytical computation with numerical simulations, finding an excellent agreement. In other words, we obtain from Replica Symmetry Breaking a faithful description of spin glasses upon varying parameters that works for random graphs and in four dimensions; currently, Replica Symmetry Breaking is the only theory that can do this.

In low-temperature spin glasses, replica symmetry breaking (RSB) theory predicts that for a given large sample, equilibrium states are non-self-averaging and organized as the leaves of a weighted random tree (1). The statistics of these trees are universal, they depend only on the overlap order parameter function $q(x)$, or equivalently, the average overlap probability distribution $P(q)$. The relative weights of the branches, proportional to the exponential of the free energies of the states, also display universal statistics, obeying the so-called Ruelle probability cascades (2–5).

Despite having first been derived in the Sherrington–Kirkpatrick (SK) model this description is completely general: It is valid in more general Mean Field models such as spin glasses on finite coordination random graphs.* If RSB is correct for finite-dimensional spin-glass systems, these predictions should be also valid in this case: A failure of these predictions would falsify RSB in its present form.

This complex statistical structure has striking consequences on the behavior of the overlap distribution function and the magnetization as a function of the external magnetic field H in the crossover region where the magnetic field scales with the system size N as $N^{-1/2}$ (the choice of the exponent $1/2$ will be justified later). We find that these quantities can be exactly computed as a function of $h = HN^{1/2}$ in the infinite volume limit: At a fixed value of h, the magnetic field $H = h/N^{1/2}$ goes to zero, consequently we call h the vanishing magnetic field.

We stress that all the analytic predictions are strictly valid in the infinite volume limit; finite volume systems will present corrections that strongly depend on the structure of the system and that are not well understood from first principles. It is clear however that these corrections should be smaller and smaller for large volumes.

Vanishing Fields. Vanishing external fields are interesting when a system has more than one equilibrium state, adding an external perturbation $\delta\mathcal{H}$ to the Hamiltonian has two effects:

*The SK model has a simple RSB solution because the free energy can be computed using a Gaussian stochastic process on the tree. This is not true in finite coordination systems, where the process is no more Gaussian and the RSB solution is more complex.

Author contributions: S.F. and G.P. designed research; M.A.-J., S.F., V.M.-M., J.M.-G., G.P., F.R.-T., and J.J.R.-L. performed research; M.A.-J., S.F., V.M.-M., J.M.-G., G.P., F.R.-T., and J.J.R.-L. analyzed data; and M.A.-J., S.F., V.M.-M., J.M.-G., G.P., F.R.-T., and J.J.R.-L. wrote the paper.

Reviewers: S.B., Emory University; and K.H., Tokyo Daigaku.

The authors declare no competing interest.

[1]To whom correspondence may be addressed. Email: miguelaj@unex.es or giorgio.parisi@roma1.infn.it.

This article contains supporting information online at https://www.pnas.org/lookup/suppl/doi:10.1073/pnas.2404973121/-/DCSupplemental.

Published September 20, 2024.

1. Change the relative weights of the equilibrium states; the interesting situation is when these effects are of $O(1)$.
2. Change the properties inside a given state.

In the ideal scenario, the external perturbation δH is strong enough to produce the effect 1), but weak enough to not produce the effect 2). Indeed, we can compute 1) from first principles, provided that we know the phase structure of the system and the value of the order parameter, while the computation of 2) requires a much deeper knowledge of the system that often is not available. Therefore the scaling with N of the perturbation should be carefully chosen to satisfy both criteria and to produce not-too-simple predictions.

Let us consider a crystal clear case: the Ising ferromagnetic model with symmetric boundary conditions (e.g., periodic boundary conditions). In this model, at low temperatures and zero magnetic field, the equilibrium Gibbs measure is the mixture of two pure states[†] with positive and negative magnetization $\pm m$ with equal weights $w_\pm = 1/2$. We can write, for an observable Ω depending on the configuration of the system:

$$\langle \Omega \rangle_G = w_+ \langle \Omega \rangle_+ + w_- \langle \Omega \rangle_- \,, \qquad [1]$$

where the two states $\pm$ are clustering (i.e., the connected correlation functions go to zero at large distances). The pure states can be obtained by adding an external field H: We have to consider first the limit where N (the total number of spins) goes to infinity and later the limit where H goes to zero. Indeed in the limit $H \to 0^{\pm}$ we obtain the state $\langle \rangle_\pm$.

All that is well known. We now introduce the vanishing field $\tilde{h} \equiv NH$ and we study what happens in the limit of $N \to \infty$ at fixed $\tilde{h}$ (we write $\tilde{h}$, rather than h, to stress the fact that these arguments refer to a ferromagnetic system; we choose $\tilde{h} > 0$ to fix the ideas). With such scaling the perturbation of the Hamiltonian is finite in typical configurations. The field is not strong enough to suppress the "-" states, but it is strong enough to modify the weights, which are now given by $w_\pm = (1 \pm \tanh(\beta \tilde{h} m))/2$, where m is the spontaneous magnetization per spin. We have a crossover behavior as a function of $\tilde{h}$, and the usual situation with only a single pure state is obtained only for $|\tilde{h}| \gg 1$.

This can be shown using perturbation theory in $\tilde{h}$, that implies that for an observable Ω,

$$\langle \exp(-\beta \delta \mathcal{H}) \Omega \rangle_\pm = \exp(\pm \beta \tilde{h} m + \frac{\beta^2 \tilde{h}^2}{2} \chi + \mathcal{O}(\tilde{h}^3/N^{1/2})) \langle \Omega \rangle_\pm \,, \qquad [2]$$

χ being the magnetic susceptibility. The effects of the vanishing field are dominated by the leading term proportional to the spontaneous magnetization m; the term $\tilde{h}^2 \chi$ is the same in both states and hence it does not change their weights.

With an eye on the spin glass case that will be considered in the next section, it may be interesting to consider as well for a ferromagnetic system the overlap between the equilibrium configurations of two replicas σ and τ

$$q = \frac{1}{N} \sum_i \sigma_i \tau_i \qquad [3]$$

The probability distribution of q can be easily computed as function of $\tilde{h}$

$$P(q; \tilde{h}) = A_+(\tilde{h}) \delta(q - m^2) + A_-(\tilde{h}) \delta(q + m^2) \,, \qquad [4]$$

$$A_\pm(\tilde{h}) = \frac{1}{2} \left(1 \pm \tanh^2(\beta \tilde{h} m) \right) \,. \qquad [5]$$

When the vanishing field $\tilde{h}$ becomes large we find $A_+(\tilde{h}) \to 1$ and $A_-(\tilde{h}) \to 0$. We can also consider the probability distribution $P_C(q; \tilde{h})$ of the "chaos overlap," i.e., the overlap between one configuration at $\tilde{h} = 0$ and another at $\tilde{h} \neq 0$. In this case, independently of $\tilde{h}$, one simply has

$$P_C(q; \tilde{h}) = \frac{1}{2} \left(\delta(q - m^2) + \delta(q + m^2) \right) \qquad [6]$$

We could also consider the effect of a random magnetic field in a ferromagnetic system: $\delta \mathcal{H} = -\hat{h}/N^{1/2} \sum_{i=1}^N r_i \sigma_i$, where the r_i are centered random variables with variance one. If we define the total magnetic field by

$$NH = \frac{\hat{h}}{N^{1/2}} \sum_{i=1}^N r_i \,, \qquad [7]$$

then the vanishing field for this random case would be $H = (z\hat{h}/N)$, where z is a Gaussian number of unit variance. In this case, we have a different power of N in the definition of the vanishing field because, in order to have a finite effect on the weights, we need a finite value of $\langle \delta \mathcal{H} \rangle_\pm$ in the infinite volume limit.

The effect of such a perturbation is slightly more subtle than the one of a constant field. In the presence of the field, the weights of the states are random variables that depend on the r_i. One needs now to define $P(q)$ averaging over the r_i: $P(q) = \overline{P_r(q)}$. A straightforward computation reveals that in this case $P(q)$ is still as in Eq. **4** but with

$$A_\pm(\hat{h}) = \frac{1}{2} \pm \frac{1}{2} \int d\mu(z) \tanh^2(\beta h z m) \,, \qquad [8]$$

where $d\mu(z)$ is a Gaussian probability distribution with unit variance and zero average.

While these results are simple and perhaps not surprising, we fear that no one has spelled them in detail. They are valid for any dimensions whenever in the low-temperature phase we have a spontaneous magnetization. It should be emphasized that this is true even in two dimensions, where any macroscopic random field destroys the ordered phase. In this marginal case perturbation theory breaks down as soon as $\hat{h} = O(N^{1/2})$ and our formulae in the vanishing field regime, give no information on the behavior when the field is $H = O(1)$.

Spin Glasses. The situation is more complex in spin-glasses in the standard RSB picture where the number of equilibrium states is infinite. When a small random perturbation is added, the Boltzmann weights of the tree's branches are reshuffled. As the intensity of the perturbation grows, states that originally had a small weight become dominant, and the overlap between the unperturbed and the perturbed system decreases. For any small but macroscopic perturbation, this implies vanishing similarity, a property known as chaotic dependence on the intensity of the perturbation (6–8).

A well-known example of chaotic behavior is chaos against temperature (9–12) where, however, a variation of temperature

[†]A state is pure if the connected correlations vanish at infinity; for translation invariant systems there are many equivalent definitions of pure states.

does not result in a random perturbation unrelated to the energy landscape (see later). Quantitative predictions are more difficult and less universal: Both kind of spin glass models—with chaos and without chaos—are known. Even in mean field models, like the SK model, where chaos is present, explicit computations have only been done near the critical temperature.[‡]

In this paper, we study the effect of a magnetic field, where the theory is simpler and chaos has universal features that are absent for temperature chaos.[§] The development of a general theory is possible here because in the absence of a field, the average magnetizations of the states are Gaussian random variables uncorrelated with the energy of the states. This generic property always holds if there are many states and random couplings without a ferromagnetic component.

The interesting zero temperature limit of the present problem, where ground-state level crossings lead to avalanche-like discontinuous jumps in the magnetization, was studied for long-range models in refs. 20–22. Using an adaptation of the replica method introduced in ref. 23 a closed formula for the avalanche density in the limit $h \to 0$ was found. Here, we are interested in finite temperatures, and also in the full dependence on the spin-glass vanishing field $h = HN^{1/2}$.[¶]

Remarkably, the predictions of standard RSB about magnetic field chaos can be submitted to a *quantitative* test, once the function $P(q)$, or equivalently $q(x)$, at zero magnetic field has been measured. Indeed, one can generate random trees and their relative weights in the absence or the presence of a field, and directly compare with the results of numerical simulations.

In this paper, we compare the theory's predictions with the simulations of two models exhibiting low-temperature spin glass behavior: the Bethe lattice spin glass and the 4D Edwards–Anderson model. Deviations from the theory can be expected either for finite-size effects or because of the absence of standard RSB. To calibrate the first effect, we study the Bethe lattice spin glass, where the standard RSB structure of the states is present (although only approximate RSB solutions are available); in this case, we find a very good agreement with the theory as expected. In a second moment, we study the 4D spin glass, where qualitatively we find very similar finite size effects. Also, in this case, the agreement is excellent, consistently with clear evidence in favor of RSB in this system at least at zero magnetic field (24–26). We are not discussing in this note the existence of RSB in the presence of a fixed nonzero magnetic field $H = \mathcal{O}(1)$. Different viewpoints exist on this separate problem, (e.g., ref. 27) which is not relevant to us because we are concerned with fields $H \sim 1/N^{1/2}$.

Broken Replica Symmetry Theory. For the reader's convenience, and to establish notations, let us recapitulate the theory using slightly imprecise but simplified language. We suppose to deal with a spin glass without a net ferromagnetic component in the couplings and invariant under spin reversal. In the RSB phase in each instance of the system, there is an infinite number of equilibrium states labeled by α. These states have random statistical weights w_α, normalized to $\sum_{\alpha=1}^{\infty} w_\alpha = 1$, magnetizations $m_\alpha = N^{-1/2} \sum_{i=1}^{N} \langle \sigma_i \rangle_\alpha$, and mutual overlaps $q_{\alpha\gamma} = N^{-1} \sum_{i=1}^{N} \langle \sigma_i \rangle_\alpha \langle \sigma_i \rangle_\gamma$, where $\langle (\cdots) \rangle_\alpha$ denotes the statistical average in the state labeled by α. The normalization of the magnetization has been chosen to have $m_\alpha = O(1)$ for large N. In fact, in each state spins freeze in random directions and the m_α are Gaussian, zero mean variables, with covariance $\langle m_\alpha m_\gamma \rangle = q_{\alpha\gamma}$. The *positive* overlaps are constrained by ultrametricity, implying that the states are organized as random trees, whose statistics we describe later.

It is convenient to define the probability distribution of the overlap for a given disorder realization (sample) $P_J(q)$ and its average:[#]

$$P_J(q) = \sum_{\alpha,\gamma} w_\alpha w_\gamma \delta(q - q_{\alpha\gamma}), \quad P(q) = \overline{P_J(q)}, \qquad [9]$$

being $\overline{(\cdots)}$ the average over the disorder. In mean-field models, $P(q)$ has a continuous component and a δ peak: $P(q) = \tilde{P}(q) + (1 - x_M)\delta(q - q_{\mathrm{EA}})$, with $x(q) = \int_0^q \mathrm{d}q' \, P(q')$ and $x(q_{\mathrm{EA}}) = x_M$. Notice that the function $q(x)$ is defined as the inverse function of $x(q)$.

We can ask now what happens to the overlap when in a given system one replica is at zero magnetic field and the other at nonzero *small* magnetic field $H = h/\sqrt{N}$ (both replicas of the system share the same disorder). In this regime one only adds a finite perturbation—keep in mind that the total magnetization is of order $\sqrt{N}$ which is the rationale for the choice of normalization in the definition of m_α. In this way, the states keep their identity, while their weights are modified: $w_\gamma \to w_\gamma(h) \propto w_\gamma \exp(\beta h m_\gamma)$ with $\sum_\gamma w_\gamma(h) = 1$. Notice that, as it is well known (3), the distribution of the weights is left invariant by such a reweighting independently of the value of h. We are interested here to the correlations between the original weights and their reweighted version. We readily find that the probability distribution of the overlap between the two replicas of the system (one in the absence and the other in presence of the field) is given by $P_{J,C}(q; h) = \sum_{\alpha,\gamma} w_\alpha w_\gamma(h) \delta(q - q_{\alpha\gamma})$, or, when both replicas of the system feel the same magnetic field, $P_J(q; h) = \sum_{\alpha,\gamma} w_\alpha(h) w_\gamma(h) \delta(q - q_{\alpha\gamma})$.

An additional grain of salt is due, because the system is invariant under spin reversal at $h = 0$. For any state α, there is a state α' with opposite magnetization and $w_{\alpha'} = w_\alpha$. It is convenient to remove this degeneracy: We use only one label for each pair of states and we define $q_{\alpha\gamma}$ such that $q_{\alpha\gamma} > 0 \; \forall(\alpha, \gamma)$. This is the convention we use in the generation of the spin glass trees. In the end, one reconstructs

$$P_J^C(|q|; h) = \sum_{\alpha,\gamma} w_\alpha w_\gamma(h) \delta(q - q_{\alpha,\gamma}), \qquad [10]$$

where now $w_\gamma(h) \propto w_\gamma \cosh(\beta h m_\gamma)$. Similarly, the probability distribution of the overlap (positive *and* negative) between two replicas in a field $P_J(\pm|q|; h)$ is:

$$P_J(\pm|q|; h) = \sum_{\alpha,\gamma} w_\alpha(h) w_\gamma(h) g_\pm(h, m_\alpha, m_\gamma) \delta(|q| - q_{\alpha\gamma}), \qquad [11]$$

with $g_\pm(h, m_\alpha, m_\gamma) = [1 \pm \tanh(\beta h m_\alpha) \tanh(\beta h m_\gamma)]/2$. Note that in the limit $h \to \infty$ [$H > 0$, fixed, while $N \to \infty$]: $P_C(|q|; \infty) = \delta(q)$, $P(q; \infty) = \theta(q) P(|q|)$.

[‡] Temperature chaos, when present, is due to the subtle energetic-entropic balance in the states, that is affected by temperature changes (13–18).

[§] The numerical study of chaos in a magnetic field was started twenty years ago in ref. 19 for the SK model.

[¶] This scaling is easy to understand at small h: Due to the randomness of the J, the model with constant H is equivalent to the model with a random bimodal H_i. In this situation in the replica approach, the magnetic field corresponds to a new term in the Hamiltonian, that is equal to $\frac{1}{2} H^2 \sum_{i=1,N} \sum_{a,b=1,n} \sigma_i^a \sigma_i^b + O(H^4)$. The coefficient of the term proportional to H^2 is of $\mathcal{O}(N)$ so this term is of $\mathcal{O}(H^2 N = h^2)$.

[#] This and the following similar equations should be thought of as holding in distribution sense in the thermodynamic limit.

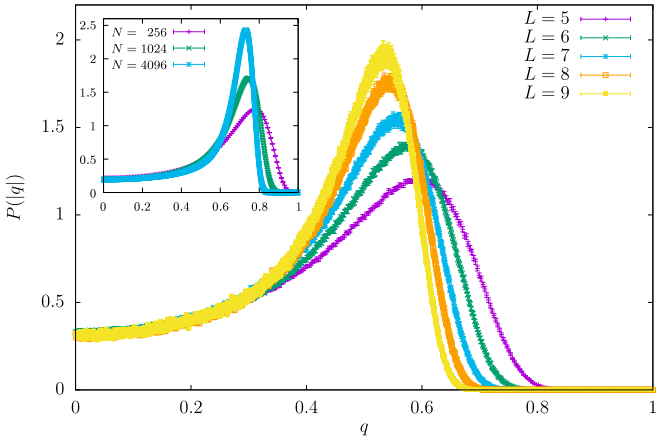

Fig. 1. The probability $P^N(|q|)$ at $h = 0$ for different values of L in 4D EA at $T = 0.7\ T_c$, $T_c(h = 0) = 2.03(3)$ (28). Notice the stable part at low q and the size-dependent peak, whose position shifts to the *Left*, while its height and width respectively increase and decrease as the system size grows. *Inset*: The probability $P^N(|q|)$ at $h = 0$ for different values of N in Bethe lattice at $T = 0.5\ T_c$, with $T_c(h = 0) \simeq 1.518651$.

An additional quantity of interest is the average magnetization induced by h; using the previous formulae we find that $m(h) = \beta h[1 - \int_{-1}^{1} \mathrm{d}q\, qP(q;h)]$ (see *SI Appendix* for details).

All these functions are nontrivial(at variance with the case of ferromagnetic systems). Remarkably, they can be computed efficiently, provided that we know the function $P(q)$ at zero magnetic field.

The simplest approach, which we follow here, is to average over a large number of random trees generated with the correct statistical properties.[‖] The reader may find a detailed explanation of how to generate RSB spin-glass trees of states with the right statistics in *Materials and methods*. Furthermore, all the technical details of the generation of the trees can be found in *SI Appendix*.

As we have stressed an input to this kind of computations is the order parameter, in the ferromagnetic case, it is m; in the RSB approach, it is $P(q)$. In the SK model, $P(q)$ can be exactly computed analytically. However, this is a lucky exception, and in general, we have to obtain $P(q)$ from numerical simulations. As explained above, the probability distributions $P(q)$, $P(q;h)$, and $P_C(q;h)$ will be the main quantities to study. To compare the theoretical predictions with the simulations, we compute those functions for the Bethe lattice and the 4D Edwards–Anderson model. The details of the computation of the probability distributions $P^N(q)$, $P^N(q;h)$, and $P_C^N(q;h)$ for different system sizes N in the simulations can be found in *Materials and methods*.

The probability distributions $P^N(q)$—as well as $P^N(q;h)$ and $P_C^N(q;h)$—have a strong dependence on N (Fig. 1), the height of the peak increases (it should go to infinity), and the position of the peak slightly drifts. Now the extrapolation to $N \to \infty$ is not easy and the results depend on the functional form of the finite volume corrections. We avoid this problem by the following trick: We suppose that the infinite volume $P(q)$ is well approximated by $P^N(q)$ and we compute $P^N(q;h)$ and $P_C^N(q;h)$ under this hypothesis. To minimize finite volume effects, instead of comparing directly the overlap probability distributions, we found it convenient to consider, for $|q| \leq q_{\mathrm{EA}}$, the ratio of the probabilities distributions of the overlaps in the presence and absence of the field

$$R_C^N(|q|;h) = \frac{P_C^N(|q|;h)}{P^N(|q|;0)}, \quad R^N(q;h) = \frac{P^N(q;h)}{P^N(q;0)}. \qquad [12]$$

A crucial prediction of RSB is that these functions R remain nontrivial in the infinite volume[**] and are equal to the one computed analytically with the procedure described above. We can compare the numerical and the theoretical values of these functions, or compare for example $P_C^N(|q|;h)$ with $P_C^N(|q|;h)$ multiplied by the analytic prediction for $R_C^N(|q|;h)$ obtained by RSB theory.

Results. The numerical and theoretical probability distributions are shown in Fig. 2 for the Bethe lattice and in Fig. 3 for the 4D EA model. In both cases, we find an excellent agreement between the theoretical predictions from the ultrametric tree and the numerical results for the functions $P_C^N(q;h)$ and $P^N(q;h)$. We also plot the numerical $P^N(q)$, which is used as an input for the theoretical prediction.

In these two figures, we show the results for the largest system we have simulated and the reader may be wondering what happens for smaller systems (because the functions $P_N(q)$ vary with N).

In order to appreciate better the quality of the comparison we find it more convenient to plot the analytic and numerical ratios $R_C^N(|q|;h)$ and $R^N(|q|;h)$. In this way, we can better appreciate the deviations from the theory in the region where the functions P's are small. The detailed results for the function $P_C^N(|q|;h)$ and for $P^N(q;h)$ are shown in *SI Appendix*.

In Fig. 4, we compare the theoretical predictions for $R_C^N(|q|;h)$ with the 4D EA computations, and also with the Bethe lattice ones (in the *Inset*). Interestingly, the ratio is a linear function of q^2 with a good approximation. The plot is done in the region $|q| <$

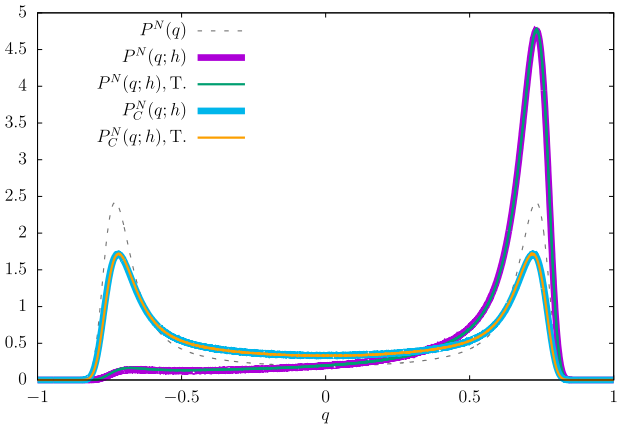

Fig. 2. The functions $P^N(q)$, $P_C^N(q;h)$, and $P^N(q;h)$ as a function of q at $T = 0.5\ T_c$ for $h = 4$ on Bethe Lattice for the largest volume simulated $N = 4{,}096$. We compare both the $P_C^N(q;h)$ and $P^N(q;h)$ curves with the predictions from the ultrametric tree (T.). The dashed line is the zero-field $P^N(q)$ function that is the input in our computation. Notice that the probability distributions $P^N(q)$, and $P_C^N(q;h)$ are fully symmetric. Therefore, in the main text, we focus the discussion on $P^N(|q|)$, and $P_C^N(|q|;h)$. The curves $P_C^N(q;h)$ and $P^N(q;h)$ have been obtained as the product of the theoretical $R^N(q;h)$ and $R_C^N(q;h)$ with the numerical $P^N(q)$.

[‖]It will be shown in a further publication how the same results could be obtained by solving partial differential equations associated with diffusion on random trees.

[**]Notice that in the limit of $T \to 0$ $R_C(q_{\mathrm{EA}},h)$ represents the "survival" probability that the ground state has not crossed in the interval of fields $[0,h]$. The expression we write here provides a natural finite temperature generalization of this survival probability.

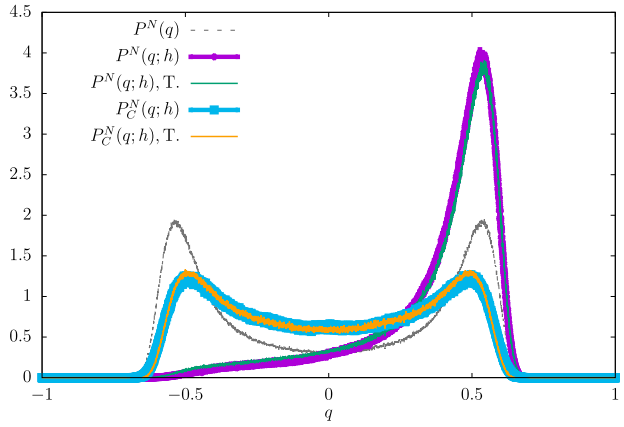

Fig. 3. The functions $P^N(q)$, $P_C^N(q;h)$, and $P^N(q;h)$ as a function of q at $T = 0.7\ T_c$ for $h = 10$ on the 4D Edwards Anderson for the largest volume simulated $N = 9^4$. We compare both the $P_C^N(q;h)$ and $P^N(q;h)$ curves with the predictions from the ultrametric tree (T.). The dashed line is the zero-field $P^N(q)$ function that is the input in our computation. Notice that the probability distributions $P^N(q)$, and $P_C^N(q;h)$ are fully symmetric. Therefore, in the main text, we focus the discussion on $P^N(|q|)$, and $P_C^N(|q|;h)$. The curves $P_C^N(q;h)$ and $P^N(q;h)$ have been obtained as the product of the theoretical $R^N(q;h)$ and $R_C^N(q;h)$ with the numerical $P^N(q)$.

$q_{\rm EA}$, where we can directly compare the data with the analytic predictions. The statistical errors increase in the region of small $|q|$ because in that region the probability $P(q)$ is smaller than in the peak. Furthermore, in Fig. 5, we compare the theoretical predictions for $R^N(|q|;h)$ with the 4D EA computations and with the Bethe lattice ones (in the *Inset*). Again, the plot is restricted to the region $|q| < q_{\rm EA}$, where we can directly compare the data with the analytic predictions. The data at negative q have stronger volume dependence. The reasons are quite clear. The theory predicts that this ratio is 1 at $h = 0$ because by continuity in H, $\text{Prob}(|q|;h) \equiv P(q;h) + P(-q;h)$ is independent of h.[††]

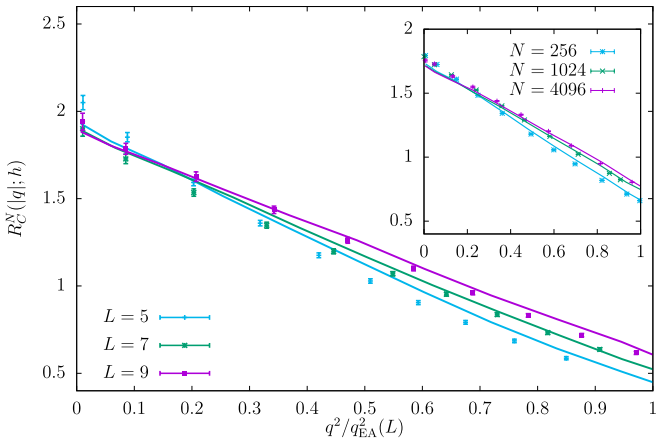

Fig. 4. The ratio $R_C^N(|q|;h)$ as a function of $q^2/q_{\rm EA}^2(L)$ at $T = 0.7\ T_c$ for $h = 10$ and different values of L in the 4D EA model. Lines correspond to the theoretical prediction from the ultrametric tree and points correspond to simulations. For visualization purposes, we have plotted only a discrete subset of values of q. *Inset*: Ratio $R_C^N(|q|;h)$ as a function of $q^2/q_{\rm EA}^2(N)$ at $T = 0.7\ T_c$ for $h = 4$ and different values of N in the Bethe lattice.

[††]This can be seen as a consequence of the invariance of the probability of the weight's distribution under the reweighting due to the field, as implied by stochastic stability; indeed also in our analytic computations the property is exactly valid only in a limit, namely $M \to \infty$ see *Materials and methods*.

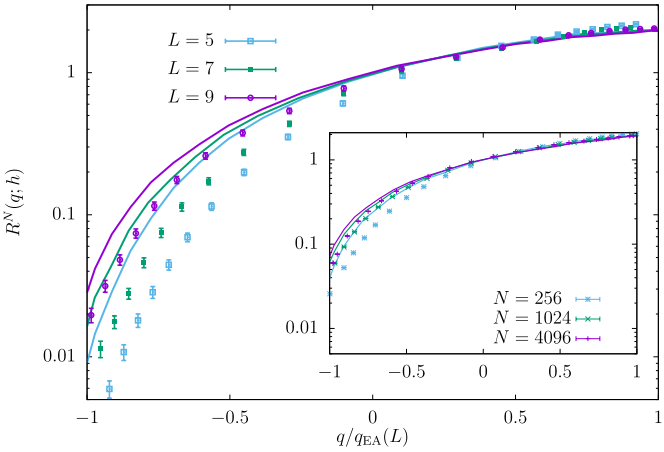

Fig. 5. The ratio $R^N(q;h)$ as a function of $q/q_{\rm EA}(L)$ at $T = 0.7\ T_c$ for different values of L in 4D EA lattice ($h = 10$). Lines correspond to the theoretical prediction from the ultrametric tree and points correspond to simulations. For visualization purposes, we have plotted only a discrete subset of values of q. *Inset*: ratio $R^N(q;h)$ as a function of $q/q_{\rm EA}(N)$ at $T = 0.5\ T_c$ for different values of N in Bethe lattice ($h = 4$).

On the other hand, for any *finite* field H, the negative values of q should have zero probability in the infinite volume limit.

Therefore the region of q near zero (and consequently also for $q < 0$) is strongly affected by finite size effects.

We see that for small sizes the analytic computations are less accurate but qualitatively correct: This should be expected as far as the analytic computations are exact only in the infinite volume limit. Moreover, the peaks are wider (Fig. 1) and the tail of the peaks sometimes arrives near zero: In this situation, our fitting procedure for the function $P(q)$ has a higher degree of approximation. The important message is that the difference between theory and numerical data strongly decreases by increasing the volume.

The asymmetry of the function $P^N(q;h)$ is evident (Figs. 2 and 3): Remember that in the limit $h \to \infty$, $P^N(q;h)$ for $q < 0$ must be zero, and $P^N(q;h) = 2P^N(q)$ for $q \geq 0$, as it happens at an arbitrary small nonzero value of H in the infinite volume limit. For finite h the two curves $P^N(q;h)$ and $P^N(q)$ cross at $q = 0$. The chaos effect can be clearly identified as a decrease of the two peaks of $P_C^N(q;h)$ at $q = \pm q_{\rm EA}$ and by an increase in the region somewhat far from the peak, in particular in the region of q near zero. Asymptotically, for large $|h|$, $P_C^N(q;h)$ should become a delta function $\delta(q)$ and we are very far away from this limit.

Finally, an important observable, that could be directly measured in experiments, is the average magnetization as a function of h that verifies:

$$m(h) = \beta h \left(1 - \int_{-1}^{1} \mathrm{d}q\ P(q;h)\ q\right). \qquad [13]$$

as shown in *SI Appendix*.

The results are presented in Fig. 6 which displays an excellent agreement between theory and simulations in both our simulated systems. Let's discuss the implication of this result for the magnetization as a function of the standard field H:

- For a very small magnetic field ($H \ll N^{-1/2}$), the magnetization is trivially given by βH.
- When $HN^{1/2}$ is of order 1, we enter the *first* nonlinear regime that is analyzed in this paper and depicted in Fig. 6.

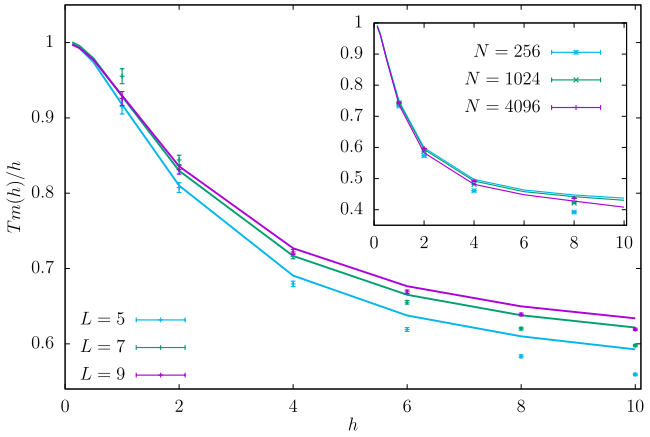

Fig. 6. $Tm(h)/h$ as a function of h for different values of L in the 4D EA lattice against the analytical prediction (continuous line) at $T = 0.7T_c$. *Inset*: $Tm(h)/h$ as a function of h for different values of N in the Bethe lattice at $T = 0.5T_c$.

- When H is small but $HN^{1/2}$ is large the magnetization per spin is given by the standard linear response formula $\beta H\left(1 - \int_0^1 \mathrm{d}q\, P(q)\, q\right)$ that is well understood, especially in solvable problems such as the SK model.
- When H is finite we enter the second nonlinear regime where the thermodynamic functions depend on the magnetic field.

Analogously to what we have seen in the ferromagnetic case, the approach of the present paper does not give information on the second nonlinear regime. We work in the regime where the function $P_N(|q|, h)$ does not depend on h and, for example, we can not get any information on the existence of a De Almeida-Thouless line and an RSB phase at a nonzero -finite- value of the magnetic field.

Discussion

We have seen that RSB theory provides universal predictions on the behavior of the system in the presence of a small random perturbation, in our case a magnetic field, that only depends on the overlap statistics at zero field. We have tested these predictions through numerical simulations of relatively small spin glass systems. The Bethe-lattice spin glass gave us an idea of how finite volume corrections modify the asymptotic results. Remarkably a very similar behavior was found in the 4D Edwards–Anderson model. This method provides further quantitative tests of the RSB predictions in this system which adds to the one of ref. 24 where one finds results in agreement with the generalized fluctuation–dissipation relations. We have seen that in the crossover region replica symmetry breaking provides zero parameters quantitative predictions of functions of two variables—the probabilities $P(q; h)$—using as a starting point only the function $P(q)$ at zero magnetic field. The excellent agreement with numerical data further hints at the correctness of the standard RSB theory in this 4D model. On the contrary, a serious disagreement between the numerical simulations and the analytic results would have falsified the correctness of the standard RSB.

Our method could have experimental relevance in laboratory spin glasses. Quantitatively testing RSB theory experimentally is notoriously difficult. In ref. 29 it has been argued that, under a suitable hypothesis of stability of the distribution of states against small but extensive perturbations (stochastic stability), the measure (30) of the modified fluctuation–dissipation relations in out of equilibrium aging dynamics (31) would directly yield access to the function $P(q)$. From this function, one could get a parameter-free prediction for the average magnetization in a small field $m(h)$. The same quantity could be obtained in direct separate measurements in well-thermalized mesoscopic samples using small-size spin-glass powders. The comparison of the measured values of the function $m(h)$ with the theoretical predictions would provide a strong consistency check of the hypothesis of ref. 29 and those of RSB theory. The interesting regime is in the *first* nonlinear regime, i.e. at fields smaller than those where the standard linear response regime works.

Chaos in a magnetic field is also an excellent alternative to temperature changes for studying memory and rejuvenation effects. This is particularly interesting because one can develop more precise theories than in the case of temperature changes.

Materials and Methods

The Tree of Spin Glasses. Let us now briefly describe how to generate RSB spin-glass trees of states with the right statistics. In spin glasses, the equilibrium measure of a given infinite volume instance is characterized by a random weighted tree of states. A tree is completely characterized by its branching points, by a set of random weights w_α of the states that are associated to the leaves α, and by the mutual overlaps $q_{\alpha\gamma}$, with $q_{\alpha\alpha} = q_{\mathrm{EA}}$. Since such trees have been discussed many times (32, 33), we will limit ourselves to a short description rather than to a full explanation.

In principle, trees have an infinite number of leaves, but by cutting off small weights, we can approximate them by trees with a finite number of leaves M. See, for example, Fig. 7.

These can be generated through a branch merging process known as Bolthausen–Sznitman coalescent (34), starting from M leaves, and progressively reducing the number of branches through a Markov process of random collisions in a "time" t. A direct branching algorithm can also be used (35), however, here we find it more convenient to use the coalescent.[‡‡]

The branching points of the tree are labeled by the time variable t ($t \geq 0$). In the following, we call nodes both the branching points and the leaves (terminal nodes). The coalescence process is ruled by the function $P(k|b) = \frac{b}{(b-1)(k-1)k}$ which tells the probability of coalescence of k nodes if at that time there are b nodes. We start with M nodes at time zero: in this case, $b = M$. We chose a number $k \in \{2, \ldots, b\}$ at random with probability $P(k|b)$ and we coalesce

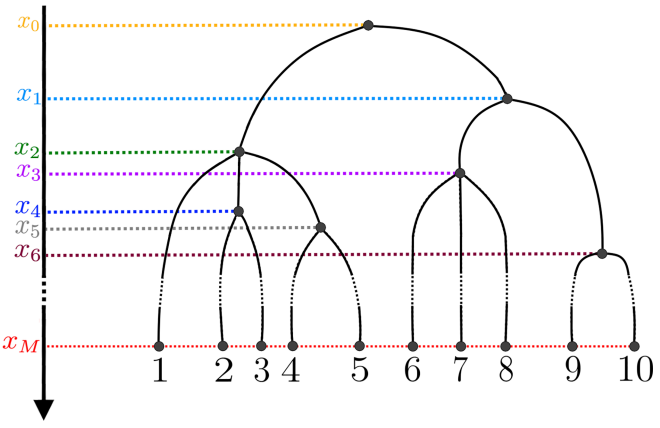

Fig. 7. A tree with ten leaves. The overlap of leave (1) with the leaves $(2 \cdots 5)$ is $q(x_2)$ and with the leaves $(6 \cdots 10)$ is $q(x_0)$; the overlaps of leave (2) with the other leaves are the same as leave (1), with the only difference that the overlap with the leave (3) is now $q(x_4)$.

[‡‡]We have run codes with both prescriptions, with identical results, but the Bolthausen–Sznitman code is simpler and more efficient.

k nodes at random into a single one. In this way b decrease to $b-k+1$. At the same moment, the time variable is incremented by a random Δt with an exponential distribution and with average $\overline{\Delta t} = 1/(b-1)$. The process stops at a finite time when $b = 1$ and no more coalescence is possible.

At each level, t is associated with a value $x(t) = x_M \exp(-t)$: The overlap between the branches that meet at that level is given by $q = q(x(t))$. This is the only point where the function $P(q)$ appears in the construction. In our case, we obtain this $P(q)$ from the numerical data (see below for further details). Once the tree is built, one needs to associate random weights to the leaves. If M is large, this is simply done by generating M i.i.d. variables u_α, for $\alpha = 1, ..., M$ with distribution $p(u) = x_M \theta(u-1) u^{-1-x_M}$, and defining the weights $w_\alpha = u_\alpha / \sum_\gamma u_\gamma$. Notice that in this construction both the weights and the overlaps associated with the given branching levels are independent of the tree's structure. The values of x_M and of $x(q)$ depend on the specific system at hand and should be given as input at the beginning of the computation.

The magnetizations m_α are zero mean Gaussian random variables with covariance $\overline{m_\alpha m_\beta} = q_{\alpha\beta}$ and they can be constructed efficiently in many ways. More details are provided in *SI Appendix*.

Comparison with Numerical Simulations. We simulate Ising spin glass models at equilibrium in their low-temperature phase. The Hamiltonian of a system with N spins in a field reads

$$\mathcal{H} = -\sum_{(i,j)\in\mathcal{E}} J_{ij} S_i S_j - \frac{h}{\sqrt{N}} \sum_{i=1}^{N} S_i, \qquad [14]$$

where $\mathcal{E}$ denotes the set of edges of the graph where the model is defined: in our case, either a Bethe lattice spin glass on a Random Regular Graph with coordination number equal to 4, or the 4D Edwards–Anderson model with periodic boundary conditions in a hypercubic lattice.

In a finite volume, the function $P(q)$ is measured as the probability distribution of the overlap between two equilibrium configurations (the replicas denoted as σ and τ) $q = \sum_i \sigma_i \tau_i / N$. We measure the probability $P(q)$ at $h = 0$ and the probabilities $P_C(|q|; h)$ and $P(q; h)$ as a function of h at low temperatures. In both cases, optimized code based on parallel tempering and multispin coding with 128 bits has been used. In Fig. 1, we show the results for the probability $P(|q|)$ for both systems at zero magnetic field.

From our numerical data, we extrapolate the functions $x(q)$ from these probability distributions at infinite volume. For each simulated volume, we approximate $P(q)$ with $P_{\rm fit}(q) = a + bq^2 + (1-x_M)\delta(q-q_{\rm EA})$: So, $x(q) = aq + bq^3/3$ and $x_M = x(q_{\rm EA})$. Then we fit the values of a and b using the data in the low q^2 region and we fix $q_{\rm EA}$ such that the mean value $\overline{\langle|q|\rangle}$ computed with $P_{\rm fit}(q)$ coincides with that obtained in the numerical simulation for that particular volume. In this way, we find that the position of the peak at that given volume is only a few percent off the estimated $q_{\rm EA}$ (*SI Appendix*). Using this representation $P_{\rm fit}(q)$ of the function $P(q)$ we have all the information to assign the weights of the leaves in the building process of the tree (see above). The predictions from the random trees have been averaged over 10^5 trees with 10^5 leaves: All the results are stable toward a variation of the number of leaves and the statistical errors are small. We concentrated our attention on $\overline{\langle|q|\rangle}$ because we know that for large values of h the magnetic susceptibility depends linearly on it (*SI Appendix*).

The reader may note that the theoretical curves of the probability distributions appearing in Figs. 2 and 3 are labeled with the superindex N which, in the theoretical case, is not associated with any size of the system. This superindex refers to the numerical curve (associated to a finite lattice with N spins) from which the $P_{\rm fit}(q)$ is obtained following the above-explained process. In particular, the value x_M used as the input in the construction of the tree depends on N and this dependence is inherited by the tree.

An alternative approach would be to extrapolate the function $P(q)$ to infinite volume and to use this extrapolated function for the analytic computation. Using no extrapolation is more robust and allows us to make predictions even for a single value of N.

There is an asymmetry between our analytical approach and the numerical simulations:

- In the analytic approach, we generate the weights of the states at $h = 0$ and we reweight them by adding a magnetic field.

  The reweighting factor may be quite large: It is a number of order $\exp\left(\beta h q_{\rm EA}^{1/2} z\right)$, where z is a Gaussian number of unit variance and zero average. Therefore states that have a small probability at $h = 0$ may become dominant at $h \neq 0$. For that reason, we have to compute states with a very small probability and this can be done by considering a sufficiently large number of states (M).
- In the numerical case, we simulate the systems both at zero and nonzero magnetic field. The reader may wonder why we do not use the Swendsen-Ferrenberg reweighting method for computing numerically the probability distributions in the presence of the field just reweighting the configurations generated by simulations at zero field. This technique works for small values of the magnetic field; however, in our case, the interesting region is for relatively large field h (e.g., 4) where the Ferrenberg–Swendsen (36) reweighting method fails unless the simulation length becomes very large.

Data, Materials, and Software Availability. The data and the scripts that generate the figures of this article can be downloaded from https://github.com/maguilarjanita/SmallFieldChaos (37). All other data are included in the manuscript and/or *SI Appendix*.

ACKNOWLEDGMENTS. We acknowledge the support of the Simons Foundation (grants No. 454941, S.F. and No. 454949, G.P.). We were partly supported as well by Grants Nos. PID2022-136374NB-C21 and PID2020-112936GB-I00, both of them funded by MCIN/AEI/10.13039/501100011033, Fondo Europeo de Desarrollo Regional (FEDER), Unión Europea (UE). This research has been supported by Italian Center for Super Computing (ICSC)–Italian Research Center on High Performance Computing, Big Data and Quantum Computing, funded by the European Union–NextGenerationEU. M.A.-J. was supported by Community of Madrid and Rey Juan Carlos University through Young Researchers program in R&D (Grant CCASSE M2737). J.M.-G. was supported by the Ministerio de Universidades and the European Union NextGeneration EU/Plan de Recuperación, Transformación y Resilienca (PRTR) through 2021 to 2023 Margarita Salas grant.

Author affiliations: [a]Departamento de Matematica Aplicada, Ciencia e Ingeniería de los Materiales y Tecnológia Electrónica, Complex Systems Group, Universidad Rey Juan Carlos, Móstoles, Madrid 28933, Spain; [b]Laboratoire de Physique Théorique et Modèles Statistiques, CNRS, Université Paris-Sud, Université Paris-Saclay, 91405 Orsay, France; [c]Departamento de Fisica Teórica, Universidad Complutense, Madrid 28040, Spain; [d]Instituto de Biocomputación y Física de Sistemas Complejos, Zaragoza 50018, Spain; [e]Departamento de Fisica Teórica, Universidad de Zaragoza, Zaragoza 50009, Spain; [f]Departamento de Física, Universidad de Extremadura, Badajoz 06006, Spain; [g]Instituto de Computación Científica Avanzada, Universidad de Extremadura, Badajoz 06006, Spain; and [h]Dipartimento di Fisica, Sapienza Università di Roma, CNR-Nanotec, Rome Unit, and Istituto Nazionale di Fisica Nucleare, Sezione di Roma1, Rome 00185, Italy

1. M. Mézard, G. Parisi, N. Sourlas, G. Toulouse, M. Virasoro, Nature of the spin-glass phase. *Phys. Rev. Lett.* **52**, 1156 (1984).
2. D. Ruelle, A mathematical reformulation of Derrida's REM and GREM. *Commun. Math. Phys.* **108**, 225 (1987).
3. M. Mézard, G. Parisi, M. Virasoro, Random free energies in spin glasses. *J. Phys. Lett.* **46**, 217–222 (1985).
4. B. Derrida, A generalization of the random energy model which includes correlations between energies. *J. Phys. Lett.* **46**, 401–407 (1985).
5. D. Panchenko, *The Sherrington-Kirkpatrick Model* (Springer, 2013), pp. 33–77.
6. A. P. Young, *Spin Glasses and Random Fields* (World Scientific, Singapore, 1998).
7. M. Ney-Nifle, A. P. Young, Chaos in a two-dimensional ising spin glass. *J. Phys. A Math. Gen.* **30**, 5311 (1997).
8. I. Kondor, On chaos in spin glasses. *J. Phys. A* **22**, L163 (1989).
9. S. R. McKay, A. N. Berker, S. Kirkpatrick, Spin-glass behavior in frustrated ising models with chaotic renormalization-group trajectories. *Phys. Rev. Lett.* **48**, 767–770 (1982).

10. A. J. Bray, M. A. Moore, Chaotic nature of the spin-glass phase. *Phys. Rev. Lett.* **58**, 57–60 (1987).
11. A. Billoire, E. Marinari, Evidence against temperature chaos in mean-field and realistic spin glasses. *J. Phys. A* **33**, L265 (2000).
12. M. Baity-Jesi *et al*., Temperature chaos is present in off-equilibrium spin-glass dynamics. *Commun. phys.* **4**, 74 (2021).
13. S. Franz, M. Ney-Nifle, On chaos in mean-field spin glasses. *J. Phys. A Math. Gen.* **28**, 2499 (1995).
14. T. Rizzo, A. Crisanti, Chaos in temperature in the Sherrington-Kirkpatrick model. *Phys. Rev. Lett.* **90**, 137201 (2003).
15. L. Fernandez, V. Martin-Mayor, G. Parisi, B. Seoane, Temperature chaos in 3D ising spin glasses is driven by rare events. *Europhys. Lett.* **103**, 67003 (2013).
16. L. A. Fernandez, E. Marinari, V. Martín-Mayor, G. Parisi, D. Yllanes, Temperature chaos is a non-local effect. *J. Stat. Mech Theory Exp.* **2016**, 123301 (2016).
17. W. K. Chen, D. Panchenko, Temperature chaos in some spherical mixed p-spin models. *J. Stat. Phys.* **166**, 1151–1162 (2017).
18. D. Panchenko, Chaos in temperature in generic 2 p-spin models. *Commun. Math. Phys.* **346**, 703–739 (2016).
19. A. Billoire, B. Coluzzi, Magnetic field chaos in the Sherrington-Kirkpatrick model. *Phys. Rev. E* **67**, 036108 (2003).
20. P. L. Doussal, M. Müller, K. J. Wiese, Avalanches in mean-field models and the Barkhausen noise in spin-glasses. *Europhys. Lett.* **91**, 57004 (2010).
21. P. Le Doussal, M. Müller, K. J. Wiese, Equilibrium avalanches in spin glasses. *Phys. Rev. B* **85**, 214402 (2012).
22. S. Franz, S. Spigler, Mean-field avalanches in jammed spheres. *Phys. Rev. E* **95**, 022139 (2017).
23. J. P. Bouchaud, M. Mézard, G. Parisi, Scaling and intermittency in burgers turbulence. *Phys. Rev. E* **52**, 3656 (1995).
24. G. Parisi, F. Ricci-Tersenghi, J. J. Ruiz-Lorenzo, Equilibrium and off-equilibrium simulations of the gaussian spin glass. *J. Phys. A Math. Gen.* **29**, 7943 (1996).
25. R. A. Baños *et al*., Thermodynamic glass transition in a spin glass without time-reversal symmetry. *Proc. Natl. Acad. Sci. U.S.A.* **109**, 6452–6456 (2012).
26. P. Charbonneau *et al*., *Spin Glass Theory and Far Beyond: Replica Symmetry Breaking after 40 Years* (World Scientific, 2023).
27. M. A. Moore, Droplet-scaling versus replica symmetry breaking debate in spin glasses revisited. *Phys. Rev. E* **103**, 062111 (2021).
28. E. Marinari, F. Zuliani, Numerical simulations of the 4D Edwards-Anderson spin glass with binary couplings. *J. Phys. A* **32**, 7447 (1999).
29. S. Franz, M. Mézard, G. Parisi, L. Peliti, Measuring equilibrium properties in aging systems. *Phys. Rev. Lett.* **81**, 1758 (1998).
30. D. Hérisson, M. Ocio, Fluctuation-dissipation ratio of a spin glass in the aging regime. *Phys. Rev. Lett.* **88**, 257202 (2002).
31. L. F. Cugliandolo, J. Kurchan, Analytical solution of the off-equilibrium dynamics of a long-range spin-glass model. *Phys. Rev. Lett.* **71**, 173–176 (1993).
32. M. Mézard, G. Parisi, N. Sourlas, G. Toulouse, M. Virasoro, Replica symmetry breaking and the nature of the spin glass phase. *J. Phys. Fr.* **45**, 843–854 (1984).
33. M. Mézard, G. Parisi, M. Virasoro, *Spin-Glass Theory and Beyond* (World Scientific, Singapore, 1987).
34. E. Bolthausen, A. S. Sznitman, On Ruelle's probability cascades and an abstract cavity method. *Commun. Math. Phys.* **197**, 247–276 (1998).
35. G. Parisi, F. Ricci-Tersenghi, D. Yllanes, Explicit generation of the branching tree of states in spin glasses. *J. Stat. Mech Theory Exp.* **2015**, P05002 (2015).
36. A. M. Ferrenberg, R. H. Swendsen, New monte carlo technique for studying phase transitions. *Phys. Rev. Lett.* **61**, 2635–2638 (1988).
37. M. Aguilar-Janita *et al*., Github repository with the data and scripts to generate the figures. https://github.com/maguilarjanita/SmallFieldChaos. Deposited 13 May 2024.